IEEE Access
Multidisciplinary ⋮ Rapid Review ⋮ Open Access Journal

Received June 16, 2020, accepted July 19, 2020, date of publication August 4, 2020, date of current version September 11, 2020.

Digital Object Identifier 10.1109/ACCESS.2020.3014256

A Novel Positioning System of UAV Based on IMA-GPS Three-Layer Data Fusion

YUAN WANG[1], GUOLIANG WEI[2], (Member, IEEE), QI GUAN[1], AND YANGYANG LIU[1]
[1]School of Optical–Electrical and Computer Engineering, University of Shanghai for Science and Technology, Shanghai 200093, China
[2]College of Science, University of Shanghai for Science and Technology, Shanghai 200093, China

Corresponding author: Guoliang Wei (guoliang.wei@usst.edu.cn)

This work was supported in part by the National Natural Science Foundation of China under Grant 61873169, and in part by the Program for Professor of Special Appointment (Eastern Scholar) at Shanghai Institutions of Higher Learning.

ABSTRACT In recent years, the positioning technology for unmanned aerial vehicle (UAV) has been developed rapidly. However, there are still challenges in terms of improving the computational efficiency, accuracy, and robustness of the algorithm for applications in fast flight with UAV. In this paper, we present a novel positioning system of UAV based on IMA-GPS (inertial measurement unit array - global positioning system) three-layer data fusion, which effectively solves the positioning problem of UAV. The first layer is the distributed filtering layer, the unscented Kalman filter serves as the local filter to process the measurements generated by each IMU in the IMA. The second layer is the IMA compensation fusion layer, the data of GPS is introduced to compensate for the deviation of the navigation results calculated by each IMU. The third layer is the GPS-IMA joint optimization layer, where the outputs of the IMA and GPS are fused to obtain the attitude, speed, and position. Simulation results show that the proposed method can realize an integrated navigation system which has low cost, high accuracy, and high computational speed, so that the performance of the UAV positioning system will be improved greatly.

INDEX TERMS IMA, unscented Kalman filter, multi-sensor data fusion, UAV positioning system.

I. INTRODUCTION

For the past few years, unmanned aerial vehicles (UAVs) have been rapidly developed and widely applied in many fields such as national defense patrol, agricultural activity, monitoring, rescue, and so on. In these applications, the real-time positioning of UAVs plays an important role. Although positioning technology has been developed for many years, it still faces many challenges when it is applied to the UAVs platform. For example, the traditional single sensor solution of positioning is difficult to meet the needs of UAV for rapid state change, high real-time, and complex environment. Compared with a single model, multi-sensor fusion technology can provide more accurate and reliable information for the system [1]–[4], so the multi-sensor information fusion technology applied to the UAVs platform has become one of the hot research topics.

Global Positioning System (GPS) is frequently used for UAV positioning and navigation around the world, it has the advantages of long-term stability and no accumulation of error, but its positioning information is greatly prone to jamming [6], [27]–[31], and it can't output the flight status of UAV in real-time due to its low sampling frequency. In addition to GPS, INS is also often used in UAV positioning. As an important measurement element in the inertial navigation system (INS), the inertial measurement unit (IMU) can obtain the acceleration and angular velocity of the carrier at a high frequency. Over the past two decades, with the rapid development of Micro-Electro-Mechanical Systems (MEMS) technology, the advantages of low cost, small size, and low power consumption of IMU are gradually highlighted, so IMU has been expanded to a much wider range of navigation applications [10]. However, an obvious disadvantage of single IMU is the accumulated errors. With the increase of time, the navigation results, which are calculated by single IMU, become more and more unreliable. Based on the advantages and disadvantages of the above two navigation ways, the integrated system composed of GPS and INS becomes a common navigation system of UAV [5], [7]–[9], [25], [32], [33]. Although GPS can reduce the influence of accumulated error to a great extent, the drift of the integrated system after a long-time operation can't be

The associate editor coordinating the review of this manuscript and approving it for publication was Edith C.-H. Ngai.

completely avoided. Besides, the UAV has high requirements on the robustness of the system during the flight, and any sensor fault in GPS or INS may cause serious consequences.

Although MEMS technology has made great progress, the application of single IMU in practice is still limited by precision and stability. A natural way to solve these problems is to design a virtual high-performance IMU, which combines the measurements of multiple low-cost IMUs. And some work has been done on this issue. Rasoulzadeh and Shahri implemented a high precision and low-cost IMU array (IMA) and combined the measurements of all gyroscopes [13]. The experiment of [13] demonstrates that the proposed method can significantly reduce the impact of noise on the measurements of angular rate and obtain a higher accuracy compared with a single IMU. In [15] Chang *et al.* presented a method that combined six identical gyroscopes to form a virtual high accuracy gyroscope. However, as in reference [15], the accelerometer measurements are not used for data fusion. An open-source Multi-IMU(MIMU) platform, which contains 18 cheap IMUs, is implemented in [16]. Skog *et al.* have conducted many tests with both accelerometers and gyroscopes, and qualitatively described the different potential gains of the MIMU system. References [17] and [18] proposed to apply an IMA to pedestrian navigation and studied the noise performance of the IMA. In [19], Skog *et al.* presented an algorithm that used a maximum likelihood estimation method to fuse the measurements of the IMA. An example of an IMA which consists of 32 IMUs is shown in Fig. 1. The above work is only for the IMA, which is neither fused with the information of other sensors nor applied to the UAV.

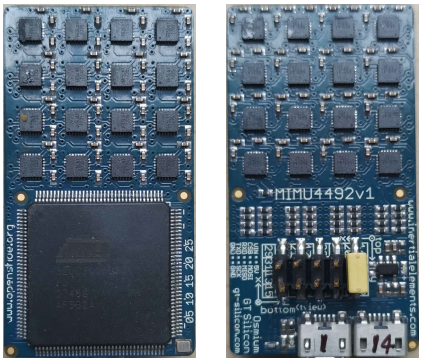

(a) Bottom side (b) Top side

FIGURE 1. An IMA consists of 32 IMUs.

In [20], [21], an effective multi-sensor fusion approach is presented and applied to INS/GNSS (global navigation satellite system) /CNS (celestial navigation system) integrated navigation system to improve the positioning performance of UAV. The method has a two-level fusion structure, the UKF serves as local filters to integrate GNSS and CNS with INS respectively to obtain the local state estimates at the bottom level, then a data fusion approach is presented to fuse the local state estimates to generate the final navigation result at the top level. GNSS and CNS, like GPS, have high measurement accuracy and good stability, but they are also prone to jamming. Moreover, compared with IMA which was not used in their work, the three sensors used in the integrated navigation system are independent of each other and have disadvantages of high cost and big size, so that they are not suitable for small-sized UAV. Also, the system state vector contains the bias of IMU in the filtering process, which increases the iteration cost and reduces the real-time performance.

Given the shortcomings of the UAV positioning system composed of GPS and INS mentioned above, we introduce IMA to replace single IMU and employ multi-sensor fusion technology to process the output of IMA and the measurements of GPS, which can improve the accuracy, robustness, and efficiency of the UAV positioning system. This paper presents a novel and multilayer data fusion methodology based on the unscented Kalman filter for IMA, which is aided by a GPS. We innovatively propose a three-layer data fusion structure, which can effectively solve the UAV positioning problem. The first layer is the distributed filter layer, and UKF serves as a local filter to process the measurements generated by IMA. UKF is used to fuse information from different IMUs in the IMA. The middle layer is the IMA compensation fusion layer, the measurement of GPS is utilized to compensate for the offset of navigation results, which are calculated by IMA. The top layer is the GPS-IMA joint optimization layer in which the navigation parameters obtained by the second layer are integrated with GPS to get the attitude, speed, and position of UAV. Besides, we calibrate the IMA before it works, and get accurate calibration parameters. Therefore, the calibration parameters do not need to be estimated in the filtering process of the UAV positioning system, and it reduces the dimension of state variables and improves the real-time performance of the UAV. The main contributions of this paper are as follows:

1) Different from some related work, the calibration parameters of the proposed system are obtained off-line rather than the on-line estimation and very accurate, therefore, it reduces the dimension of state variables and improves the realtime performance of the UAV.

2) IMA is introduced into the UAV positioning system to replace the single IMU model, which greatly enhanced the accuracy and stability of the system.

3) A three-layer data fusion structure is proposed to eliminate the accumulated errors of IMA and obtain accurate positioning results.

The rest of this paper is organized as follows. The details of the presented method are described in section II. In section III, the simulation experiment is introduced and discussed. Finally, the conclusions of this study are described in section IV.

II. ALGORITHM DESCRIPTION

In this section, we give the details of the algorithm which fuses measurements from both GPS and IMA with UKF for the UAV positioning system.

The proposed data fusion algorithm framework of GPS-aided IMA for the UAV positioning system is shown in Fig. 2. The framework has three layers, which are the distributed filtering layer, the IMA compensation fusion layer, and the GPS-IMA joint optimization layer. At the distributed filtering layer, the UKF serves as the local filter to process the measurements generated by each IMU in the IMA to obtain the local optimal state estimates. At the IMA compensation fusion layer, the measurements of GPS are introduced to compensate for the accumulated error of each local filter. Then, IMA global data fusion is performed to merge the results of IMA local data fusion into one. At the GPS-IMA joint optimization layer, the output of IMA global data fusion is fused with GPS to obtain the optimal system state, i.e. the attitude, speed, and position, which is called heterogeneous sensor data fusion.

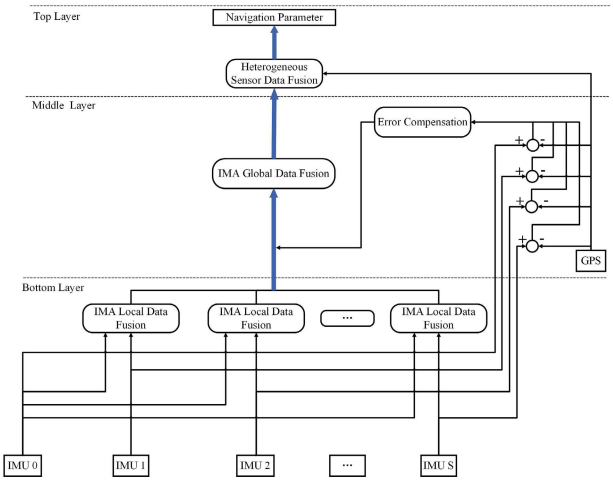

FIGURE 2. The proposed data fusion algorithm framework of GPS-aided IMA for UAV positioning system.

The navigation frame (n-frame) is chosen as the E-N-U(East-North-Up) geography frame (g-frame), moreover, i, e, b denote the inertial frame, the earth frame, and the body frame, respectively.

A. OFF-LINE CALIBRATING THE IMA

The output of the IMA which consists of S + 1 IMUs can be described by the model [22]

$$\begin{cases} \tilde{f}^{b_j} = \begin{cases} [\bar{K}_A]^i[\bar{A}]^i f^{b_i} + \nabla^{b_i} + v^i, & \text{if } j = i \\ [\bar{K}_A]^j[\bar{A}]^j\left[\bar{\xi}_A^{(j)}\right]_\times \bar{R}_{(i)}^{(j)} f^{b_i} + \nabla^{b_j} + v^j, & \text{otherwise} \end{cases} \\ \tilde{\omega}_{ib}^{b_j} = \begin{cases} [\bar{K}_G]^i[\bar{G}]^i \omega_{ib}^{b_i} + \varepsilon^{b_i} + v^i, & \text{if } j = i \\ [\bar{K}_G]^j[\bar{G}]^j\left[\bar{\xi}_G^{(j)}\right]_\times \bar{R}_{(i)}^{(j)} \omega_{ib}^{b_i} + \varepsilon^{b_j} + v^j, & \text{otherwise} \end{cases} \end{cases} \quad (1)$$

where $\tilde{f}^{b_j} \in \mathbb{R}^3$ and $\tilde{\omega}_{ib}^{b_j} \in \mathbb{R}^3$ are the measurements (linear acceleration and angular velocity) of j-th ($j = 1, 2, \cdots, S+1$) IMU. $\left[\bar{K}_A\right]^i = [I + \delta K_A]^i$, $\left[\bar{K}_G\right]^i = [I + \delta K_G]^i$, I is the identity matrix. $[\delta K_A]^i$ and $[\delta A]^i$ denote the scale factor error matrix and the sensitivity axis nonorthogonality matrix of the i-th ($i = 1, 2, \cdots, S + 1$) accelerometer. Similarly, $[\delta K_G]^i$ and $[\delta G]^i$ denote the scale factor error matrix and the sensitivity axis nonorthogonality matrix of the i-th gyroscope, respectively. f^{b_i} and ∇^{b_i} are the true specific force and bias of the i-th accelerometer in the b-frame. $\omega_{ib}^{b_i}$ and ε^{b_i} are the true angular velocity and bias of the i-th gyroscope in the b-frame. $[\xi_A^{(j)}]_\times$ and $[\xi_G^{(j)}]_\times$ denote the alignment errors in the mounting of the j-th IMU. $\bar{R}_{(i)}^{(j)} \in \mathbb{SO}^3$ represents the rotation matrix which describes the orientation from the i-th IMU to the j-th IMU. v^j is Gaussian white noise.

We calibrate the IMA offline by using the method which is provided by [22] to get the calibration parameters before it works. The calibration parameters include the accelerometer scale factors δK_{Ax}, δK_{Ay}, δK_{Az}, the accelerometer sensitivity axis nonorthogonality δA_x, δA_y, δA_z, the accelerometer biases ∇_x, ∇_y, ∇_z, the gyroscope scale factors δK_{Gx}, δK_{Gy}, δK_{Gz}, the gyroscope sensitivity axis nonorthogonality δG_x, δG_y, δG_z, the gyroscope biases ε_x, ε_y, ε_z and the alignment errors ξ_x, ξ_y, ξ_z in the mounting of each IMU, where x, y, z denote three axes of an IMU. The expressions of these parameters are as follows,

$$\begin{cases} [\delta K_A] = \begin{bmatrix} \delta K_{Ax} & 0 & 0 \\ 0 & \delta K_{Ay} & 0 \\ 0 & 0 & \delta K_{Az} \end{bmatrix} \\ [\delta A] = \begin{bmatrix} 0 & \delta A_z & -\delta A_y \\ -\delta A_z & 0 & \delta A_x \\ \delta A_y & -\delta A_x & 0 \end{bmatrix} \\ [\delta K_G] = \begin{bmatrix} \delta K_{Gx} & 0 & 0 \\ 0 & \delta K_{Gy} & 0 \\ 0 & 0 & \delta K_{Gz} \end{bmatrix} \\ [\delta G] = \begin{bmatrix} 0 & \delta G_z & -\delta G_y \\ -\delta G_z & 0 & \delta G_x \\ \delta G_y & -\delta G_x & 0 \end{bmatrix} \\ \nabla = [\, \nabla_x \quad \nabla_y \quad \nabla_z \,]^T \\ \varepsilon = [\, \varepsilon_x \quad \varepsilon_y \quad \varepsilon_z \,]^T \\ \xi = [\, \xi_x \quad \xi_y \quad \xi_z \,]^T \end{cases}$$

The IMA is placed inside the Platonic solid and the calibration parameters are obtained with the maximum likelihood estimation approach. Because the position constraints between each IMU are rigid in the IMA, which limits the navigation drift accumulated over propagation. Therefore, the calibration parameters don't need to be added to the state vector, so the computation complexity is reduced, and the computer resources are saved.

B. THE DISTRIBUTED FILTERING LAYER

The bottom layer is called the distributed filter layer which processes all accelerations and angular velocities generated by the IMA in a distributed manner. First, any IMU in the IMA is selected as the reference IMU to be used as the reference of each local filter. Second, due to the advantages of high convergence rate and high estimation accuracy, UKF is used to fuse the measurement data of each IMU and reference IMU

according to the array characteristics of IMA. Finally, the results of each local filter are fed into the IMA compensation fusion layer to complete the following steps.

Our system is similar to [26], the state vector of each local filter can be described as

$$X(t) = [\varphi_E, \varphi_N, \varphi_U, \delta V_E, \delta V_N, \delta V_U, \delta L, \delta\lambda, \delta h]^T \quad (2)$$

where, $[\varphi_E, \varphi_N, \varphi_U]^T$ and $[\delta V_E, \delta V_N, \delta V_U]^T$ are the attitude error and velocity error of the UAV in the East-North-Up directions, $[\delta L, \delta\lambda, \delta h]^T$ denotes the latitude error, longitude error, and altitude error of the UAV, respectively. The nonlinear system model of each local filter can be formulated as

$$\begin{cases} \dot{\varphi} = \varphi \times \omega_{in}^n + \delta\omega_{in}^n - C_b^n([\delta K_G] + [\delta G])\omega_{ib}^b - \varepsilon^n \\ \delta\dot{V}^n = -\varphi^n \times f^n + C_b^n([\delta K_A] + [\delta A])f^b + \delta V^n \\ \qquad \times(2\omega_{ie}^n + \omega_{en}^n) + V^n \times (2\delta\omega_{ie}^n + \delta\omega_{en}^n) + \nabla^n \\ \delta\dot{L} = \dfrac{\delta V_N}{R_M + h} - \delta h \dfrac{V_N}{(R_M + h)^2} \\ \delta\dot{\lambda} = \dfrac{\delta V_E}{R_N + h}\sec L + \delta L \dfrac{V_E}{R_N + h}\tan L \sec L \\ \qquad - \delta h \dfrac{V_E}{R_N + h} \\ \delta\dot{h} = \delta V_U \end{cases} \quad (3)$$

where $\varphi = [\varphi_E, \varphi_N, \varphi_U]^T$ and $\delta V = [\delta V_E, \delta V_N, \delta V_U]^T$; C_b^n is the 3×3 rotation matrix describing the rotation from b-frame to n-frame. ω_{in}^n is the relative rotational angular velocity between the i-frame and the n-frame, which is expressed in the n-frame. ε^n is the bias of the gyro, and ∇^n is the bias of the accelerometer. f^n is the true specific force. ω_{ie}^n is the rotational angular rate of the earth. ω_{en}^n is the relative rotational angular velocity between the e-frame and the n-frame. $\delta\omega_{ie}^n$ and $\delta\omega_{en}^n$ denote the corresponding errors. R_M and R_N represent the median radius and normal radius where the UAV locates. L, λ, h are the latitude, longitude, and altitude of the UAV.

Some key parameters in (3) can be calculated by the following equation [26]

$$\begin{cases} C_b^n = \begin{bmatrix} c\gamma c\psi + s\gamma s\psi s\theta & s\psi c\theta & s\gamma c\psi - c\gamma s\psi s\theta \\ -c\gamma s\psi + s\gamma c\psi s\theta & c\psi c\theta & -s\gamma s\psi - c\gamma c\psi s\theta \\ -s\gamma c\theta & s\theta & c\gamma c\theta \end{bmatrix} \\ \omega_{ie}^n = [\,0 \quad \omega_{ie}cL \quad \omega_{ie}sL\,]^T \\ \delta\omega_{ie}^n = [\,0 \quad \delta L\omega_{ie}sL \quad \delta L\omega_{ie}cL\,]^T \\ \omega_{en}^n = [\,-\dfrac{V_N}{R_M + h} \quad \dfrac{V_E}{R_N + h} \quad \dfrac{V_E}{R_N + h}tL\,]^T \\ \delta\omega_{en}^n = \begin{bmatrix} -\dfrac{\delta V_N}{R_M + h} + \delta h \dfrac{\delta V_N}{(R_M + h)^2} \\ \dfrac{\delta V_E}{R_N + h} - \delta h \dfrac{V_E}{(R_N + h)^2} \\ \dfrac{\delta V_E}{R_N + h}tL + \delta L \dfrac{V_E}{(R_N + h)(c^2 L)} - \delta h \dfrac{V_E tL}{(R_N + h)^2} \end{bmatrix} \\ R_M = R_e(1 - 2e + 3es^2 L) \\ R_N = R_e(1 + es^2 L) \end{cases} \quad (4)$$

where c denotes cosine, s denotes sine functions, and t denotes tangent functions. R_e and e are the semi-major axis and ellipticity of the ellipsoid model of the earth, respectively. ψ, θ, γ represent the yaw, pitch, and roll angles.

Equation (4) can be rewritten as the following standard equation of state

$$\dot{X}(t) = \bar{f}(X(t)) + B(t)u(t) + w(t) \quad (5)$$

where $\bar{f}(\cdot)$ is a nonlinear state transition function with continuous form, $B(t)u(t)$ is the control input of the system, $w(t)$ is the process noise.

The IMU samples the measurements $\tilde{f}^b$ and $\tilde{\omega}_{ib}^b$ with a period T, and these measurements are used for state propagation in the UKF. To deal with discrete-time measurements from the IMU, we apply an improved Euler formula for (5) to propagate the estimated IMU state [23]. The discrete-time model of the system state equation can be described as

$$X(k) = f(X(k-1)) + B(k-1)u(k-1) + w(k-1) \quad (6)$$

where $f(\cdot)$ is a nonlinear state transition function with discrete form. $w(k-1)$ is the process noise which is commonly assumed as a zero-mean Gaussian white noise with covariance $Q(k-1) > 0$.

The measurement model of the s-th ($s = 1, 2, \cdots, S$) local filter is described as

$$Z_s(k) = H_s(k)X(k) + v_s(k) \quad (7)$$

where $Z_s(k) = [\phi_{Eref} - \phi_{Ej}, \phi_{Nref} - \phi_{Nj}, \phi_{Uref} - \phi_{Uj}, V_{Eref} - V_{Ej}, V_{Nref} - V_{Nj}, V_{Uref} - V_{Uj}, P_{Nref} - P_{Nj}, P_{Eref} - P_{Ej}, h_{ref} - h_j]^T$. $[\phi_{Eref}, \phi_{Nref}, \phi_{Uref}]^T$, $[V_{Eref}, V_{Nref}, V_{Uref}]^T$ and $[P_{Eref}, P_{Nref}, h_{ref}]^T$ are the attitude, velocity and position of the UAV, these navigation parameters are calculated by the reference IMU. On the other hand, $[\phi_{Ej}, \phi_{Nj}, \phi_{Uj}]^T$, $[V_{Ej}, V_{Nj}, V_{Uj}]^T$ and $[P_{Ej}, P_{Nj}, h_j]^T$ are calculated by the j-th IMU. We take the difference between these navigation parameters which are obtained by these two IMUs as the measurement of the local filter. The measurement matrix is defined as $H_s(k) = diag([ones(1, 6), R_M, R_N \cos L, 1])$, $ones(1, 6)$ denotes a six-dimensional vector whose elements are all 1. $v_s(k)$ is the measurement noise which is commonly assumed as a zero-mean Gaussian white noise with covariance $R_s(k) > 0$.

The s-th local state is denoted as X_s, and the process of the s-th local filter can be described as follows:

Step 1: Initialization

$$\begin{cases} \hat{X}_s(0) = E\,[X_s(0)] \\ P_s(0) = E\left[(X_s(0) - \hat{X}_s(0))(X_s(0) - \hat{X}_s(0))^T\right] \end{cases} \quad (8)$$

Step 2: Calculate $2n + 1$ sigma points at time $k - 1$ as

$$\begin{cases} \chi_{(j,k-1)}^{(0)} = \hat{X}_s(k-1), \quad j = 0 \\ \chi_{(j,k-1)}^{(s)} = \hat{X}_s(k-1) + \gamma(\sqrt{P_s(k-1)})_j, \\ \qquad\qquad j = 1, 2, \cdots, n \\ \chi_{(j,k-1)}^{(s)} = \hat{X}_s(k-1) - \gamma(\sqrt{P_s(k-1)})_{j-n}, \\ \qquad\qquad j = n+1, n+2, \cdots, 2n \end{cases} \quad (9)$$

where $\gamma = \sqrt{n+\lambda}, \lambda = \alpha^2(n+\kappa)-n, \kappa = 3-n, \alpha$ is a tuning parameter which is a small positive value. $(\sqrt{P_s(k-1)})_j$ is the j-th column of the square root obtained by the lower triangle decomposition of the matrix $P_s(k-1)$, which is an n-dimensional column vector.

Step 3: Calculate the value of the one-step prediction model at time k as

$$\chi^{(s)}_{(j,k/k-1)} = f(\chi^{(s)}_{(j,k-1)}) + B(k-1)u(k-1), \quad j = 0, 1, 2, \cdots, 2n \tag{10}$$

$$\hat{X}_s(k/k-1) = \sum_{j=0}^{2n} W_j^{(m)} \chi^{(s)}_{(j,k/k-1)} \tag{11}$$

$$P_s(k/k-1) = \sum_{j=0}^{2n} W_j^{(c)} \left[\chi^{(s)}_{(j,k/k-1)} - \hat{X}_s(k/k-1)\right] \times \left[\chi^{(s)}_{(j,k/k-1)} - \hat{X}_s(k/k-1)\right]^T + Q_s(k-1) \tag{12}$$

where,

$$W_0^{(m)} = \frac{1}{n+\lambda}$$
$$W_0^{(c)} = \frac{\lambda}{n+\lambda} + 1 - \alpha^2 + \beta$$
$$W_j^{(m)} = W_j^{(c)} = \frac{1}{2(n+\lambda)}, \quad j = 1, 2, \cdots, 2n$$

The value of β is related to the distribution form of X_s.

Step 4: Calculate the augmented sigma points of one-step prediction model at time k as

$$\begin{cases} \tilde{\chi}^{(s)}_{(j,k/k-1)} = \hat{X}_s(k/k-1), & j = 0 \\ \tilde{\chi}^{(s)}_{(j,k/k-1)} = \hat{X}_s(k/k-1) + \gamma(\sqrt{P_s(k/k-1)})_j, & j = 1, 2, \cdots, n \\ \tilde{\chi}^{(s)}_{(j,k/k-1)} = \hat{X}_s(k/k-1) - \gamma(\sqrt{P_s(k/k-1)})_{j-n}, & j = n+1, n+2, \cdots, 2n \end{cases} \tag{13}$$

Step 5: Measurement update

$$\mathbb{Z}^{(s)}_{(j,k/k-1)} = H_s(k)(\tilde{\chi}^{(s)}_{(j,k/k-1)}) \tag{14}$$

$$\hat{Z}_s(k/k-1) = \sum_{j=0}^{2n} W_j^{(m)} \mathbb{Z}^{(s)}_{(j,k/k-1)} \tag{15}$$

$$P_s(\hat{Z}_s(k/k-1)) = \sum_{j=0}^{2n} W_j^{(m)} \left[\mathbb{Z}^{(s)}_{(j,k/k-1)} - \hat{Z}_s(k/k-1)\right] \times \left[\mathbb{Z}^{(s)}_{(j,k/k-1)} - \hat{Z}_s(k/k-1)\right]^T + R_s(k) \tag{16}$$

Step 6: Calculate the state estimate and error covariance matrix as

$$P_s(\hat{X}_s(k/k-1)\hat{Z}_s(k/k-1)) = \sum_{j=0}^{2n} W_j^{(c)} \left[\tilde{\chi}^{(s)}_{(j,k/k-1)} - \hat{X}_s(k/k-1)\right]\left[\mathbb{Z}^{(s)}_{(j,k/k-1)} - \hat{Z}_s(k/k-1)\right]^T \tag{17}$$

$$K_s(k) = P_s(\hat{X}_s(k/k-1)\hat{Z}_s(k/k-1))P_s^{-1}(\hat{Z}_s(k/k-1)) \tag{18}$$

$$\hat{X}_s(k) = \hat{X}_s(k/k-1) + K_s(k)(Z_s(k) - \hat{Z}_s(k/k-1)) \tag{19}$$

$$P_s(k) = P_s(k/k-1) - K_s(k)P_s(\hat{Z}_s(k/k-1))K_s^T(k) \tag{20}$$

Step 7: Return to step 2 for the next sample until all samples are processed.

Each IMU in IMA except the reference one independently performs the above steps to obtain the estimation of the local optimal state $\hat{X}_s(k)(s = 1, 2, \cdots, S)$ and the error covariances $\hat{P}_s(k)$.

C. THE IMA COMPENSATION FUSION LAYER

The local filter based on IMU can improve the positioning accuracy, but it can't reduce the accumulated error, which is the biggest drawback in step positioning. With the increase of time, this kind of drift error will make the state estimation deviate from the real value gradually. To solve this problem, the measurements of GPS are introduced to compensate for the influence of accumulated error on the system. According to the above analysis, the IMA compensation fusion layer is established, which is also the second layer in our framework.

First of all, we introduce the measurements of GPS, which are subtracted from the navigation parameters calculated by each IMU to acquire the corresponding error of every IMU, then we take the average of the $S+1$ errors to compensate for the fusion result of the IMA. Because GPS can't provide the attitude information, the measurements of GPS can only compensate for the velocity and position obtained by IMA. However, our experiments show that the drift of gyroscope is very small after being calibrated. The error compensated for IMA can be represented as,

$$\Delta Y = \Big((\tilde{Y}_{IMU0} - \tilde{Y}_{GPS}) + (\tilde{Y}_{IMU1} - \tilde{Y}_{GPS}) + \cdots + (\tilde{Y}_{IMUS} - \tilde{Y}_{GPS})\Big)/(S+1) \tag{21}$$

where $\Delta Y = [\Delta V_E, \Delta V_N, \Delta V_U, \Delta L, \Delta\lambda, \Delta h]^T$ is the state error compensated by GPS to the IMA. $\tilde{Y}_{IMUi} = [\tilde{V}_{EIMUi}, \tilde{V}_{NIMUi}, \tilde{V}_{UIMUi}, \tilde{L}_{IMUi}, \tilde{\lambda}_{IMUi}, \tilde{h}_{IMUi}]^T, (i = 0, 1, \cdots, S)$ is the navigation parameter which is obtained from the i-th IMU. In addition, $\tilde{Y}_{GPS} = [\tilde{V}_{EGPS}, \tilde{V}_{NGPS}, \tilde{V}_{UGPS}, \tilde{L}_{GPS}, \tilde{\lambda}_{GPS}, \tilde{h}_{GPS}]^T$ is the navigation parameter which is obtained from GPS.

Secondly, to improve the robustness of the system and reduce the impact of a single local filter fault on the system, we take the mean value of all filter results in IMA, and this can also further improve the system accuracy.

$$\hat{Y}_{IMA} = \Big((\tilde{Y}_{IMU1} - \hat{X}_1) + (\tilde{Y}_{IMU2} - \hat{X}_1) + \cdots + (\tilde{Y}_{IMUS} - \hat{X}_S)\Big)/S \tag{22}$$

where $\hat{Y}_{IMA}$ represents the state of the UAV which is the fusion result of the IMA before the error compensation.

Finally, the fusion result of this layer, $Y^*_{IMA} = [V^*_{EIMA}, V^*_{NIMA}, V^*_{UIMA}, L^*_{IMA}, \lambda^*_{IMA}, h^*_{IMA}]^T$, which eliminates the

accumulated error can be described as follows,

$$Y^*_{IMA} = \hat{Y}_{IMA} - \Delta Y \tag{23}$$

D. THE GPS-IMA JOINT OPTIMIZATION LAYER

After error compensation, the positioning accuracy of IMA fusion results is greatly improved. However, as time goes on, the accuracy of the positioning result outputted by the IMA compensation fusion layer will still slightly decrease, which is related to the sensor properties of the IMU itself. In consideration of this problem, the compensated IMA fusion results are combined with the measurements of GPS to optimize jointly by UKF, which is called the heterogeneous sensor data fusion method of the top layer, i.e. the content of GPS-IMA joint optimization layer.

Firstly, similar to the state-space model in the local filter, the state-space model in the joint optimization layer is constructed as follows.

The state vector of the joint optimization layer, which is similar to the description of the state vector of the local filter but without the attitude, is defined as

$$X'(t) = [\,\delta V'_E \quad \delta V'_N \quad \delta V'_U \quad \delta L' \quad \delta\lambda' \quad \delta h'\,]^T \tag{24}$$

Equation (4) erasing the attitude variable can be transformed into the discrete-time process model of the X',

$$X'(k) = f'(X'(k-1)) + B'(k-1)u'(k-1) + w'(k-1) \tag{25}$$

Also similar to the measurement model of the local filter, the measurement model of the joint optimization layer can be described as

$$Z'(k) = H'(k)X'(k) + v'(k) \tag{26}$$

where, $Z'(k) = \left[V^*_{EIMA} - \tilde{V}_{EGPS}, V^*_{NIMA} - \tilde{V}_{NGPS}, V^*_{UIMA} - \tilde{V}_{UGPS}, P^*_{NIMA} - \tilde{P}_{NGPS}, P^*_{EIMA} - \tilde{P}_{EGPS}, h^*_{IMA} - \tilde{h}_{GPS}\right]^T$. $\left[\tilde{V}_{EGPS}, \tilde{V}_{NGPS}, \tilde{V}_{UGPS}\right]^T$ and $\left[\tilde{P}_{NGPS}, \tilde{P}_{EGPS}, \tilde{h}_{GPS}\right]^T$ are the velocity and position of the UAV, which are provided by GPS. $\left[V^*_{EIMA}, V^*_{NIMA}, V^*_{UIMA}\right]^T$ and $\left[P^*_{NIMA}, P^*_{EIMA}, h^*_{IMA}\right]^T$ are the velocity and position of the UAV, which are provided by the IMA after error compensation. The measurement matrix is $H'(k) = diag\,([ones(1, 3), R_M, R_N \cos L, 1])$.

Secondly, the state-space model composed of (25) and (26) is substituted into the (8)–(20) to obtain the global optimal state estimation $\hat{X}'$ and the corresponding navigation parameter is

$$Y^* = \tilde{Y} - \hat{X}' \tag{27}$$

where $\tilde{Y}$ denotes the measured navigation parameter.

Finally, the attitude estimates in $\hat{Y}_{IMA}$ obtained from the IMA compensation fusion layer is added to Y^*.

$$Y^* \leftarrow \left[\,\hat{\phi}_{EIMA} \quad \hat{\phi}_{NIMA} \quad \hat{\phi}_{UIMA} \quad Y^*\,\right]^T \tag{28}$$

Thus, the augmented Y^* is the output of the GPS-IMA joint optimization layer, i.e. the navigation parameters outputted by the whole UAV positioning system.

III. SIMULATION

In this section, the effectiveness of the proposed positioning system is verified via the datasets. And comparative simulation shows that our method can provide more accurate and reliable positioning results for UAV.

A. DATASETS

According to the specifications of IMU and GPS which are provided by the sensor manufacturers, the datasets are generated by numerical simulation. Note that, we assume that all the measurements from the sensors have been synchronized. The experimental navigation data is selected from the datasets within a continuous period of 600s, which includes a variety of maneuvers, such as climbing, turning, accelerating, decelerating, pitching, rolling, etc., as shown in Fig. 3. The number of IMUs in the IMA is set to 5, and the number of samples is 60000.

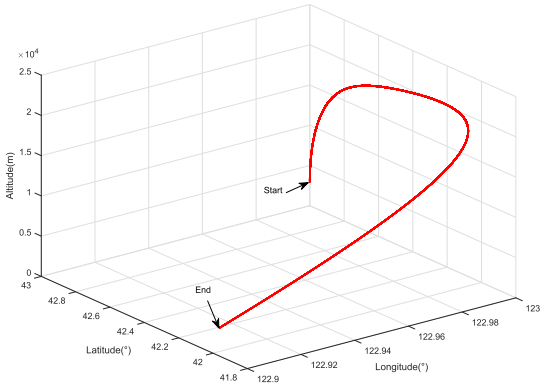

FIGURE 3. Flight trajectory of the UAV.

B. COMPARATIVE SIMULATION ON DATASETS

1) CALCULATION OF CALIBRATION PARAMETERS OF IMA

As shown in Fig. 1 and Fig. 4, a real IMA was employed for the calibration experiment using the method proposed in [11], [22]. The IMA was placed inside the calibration device. And the calibration parameters obtained are shown in Table 1, where $\left[\bar{K}_A\right] \approx \left[\bar{K}_G\right]$, $[\delta A] \approx [\delta G]$, $\left[\bar{\xi}^{(j)}_A\right]_\times \approx \left[\bar{\xi}^{(j)}_G\right]_\times$.

FIGURE 4. The calibration device.

The ground truth in the datasets and the calibration parameters in Table 1 are used to generate the digital simulation measurements of IMA.

TABLE 1. Calibration parameter.

$cali\_param$	1	2	3	4	5
K_{Ax}	0.997512	0.996088	0.996988	0.997547	0.996405
K_{Ay}	0.99996	0.997854	0.999626	0.999938	1.000411
K_{Az}	1.005537	1.01238	1.006043	1.007016	1.001638
$\nabla_x[m/s^2]$	-0.10427	-0.21078	-0.20682	-0.30518	-0.14069
$\nabla_y[m/s^2]$	0.325302	0.166577	0.294312	0.11771	0.371709
$\nabla_z[m/s^2]$	-0.12096	0.011041	0.05591	0.325742	0.034028
$\delta A_x[rad]$	-0.00132	-3.09E-05	-0.00343	-0.00082	-0.0034
$\delta A_y[rad]$	-0.00366	2.23E-05	-0.00118	0.00252	0.002145
$\delta A_z[rad]$	-0.00534	0.00544	-0.00239	0.000897	0.003183
$\xi_{Ax}[rad]$	0	0.001538	-0.00496	0.000961	-0.00269
$\xi_{Ay}[rad]$	0	-0.00266	0.001218	0.00183	0.002173
$\xi_{Az}[rad]$	0	-0.00375	-0.00217	-0.00522	0.000744
$\varepsilon_x[rad/s]$	-0.50962	-0.19083	1.385679	-0.69993	-1.31158
$\varepsilon_y[rad/s]$	-0.39078	-0.53295	-0.07615	-0.4628	-0.65598
$\varepsilon_z[rad/s]$	0.182876	-1.12176	0.129852	-0.40753	0.840208

To illustrate the importance of calibration, the calibration results of a single IMU are attached here. Due to the space limitation, the pitch error, east velocity error, and east position error before and after the calibration of IMU0 are shown in Fig. 5-7.

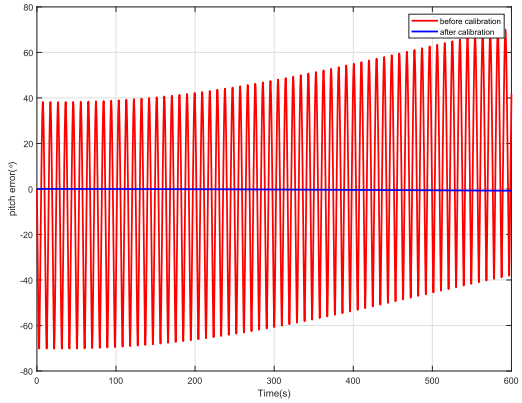

FIGURE 5. Comparison of pitch angle errors before and after the calibration of IMU0.

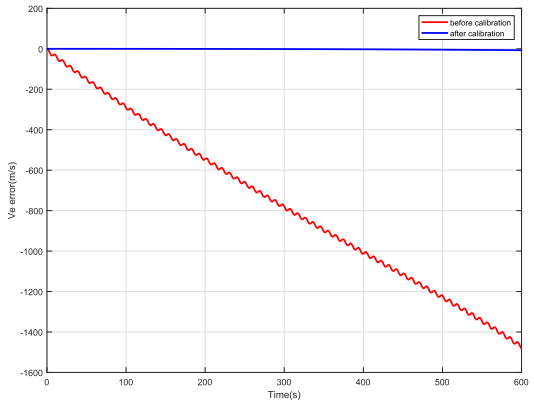

FIGURE 6. Comparison of east velocity errors before and after the calibration of IMU0.

From the above three figures, it can be seen that the attitude angle, velocity, and position of the single-IMU will become very unreliable with the increase of time, if it is not calibrated. For example, after the calibration, the drift of the east position at 10s is reduced from 215m to 0.04731m compared with that before the calibration. Therefore, the subsequent experimental data are all based on the measurements after the calibration of the IMA.

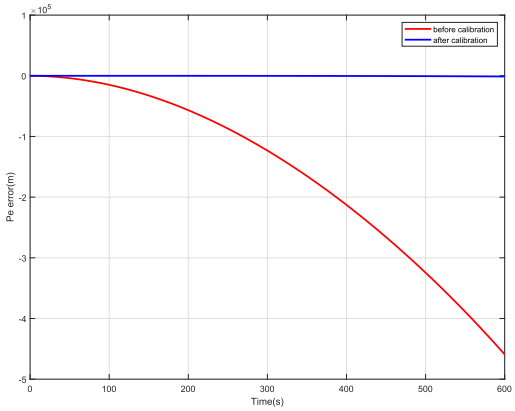

FIGURE 7. Comparison of east position errors before and after the calibration of IMU0.

2) COMPARISON OF THE PERFORMANCE OF THE CALIBRATED IMA AND THAT OF THE CALIBRATED SINGLE IMU

In this subsection, the calibrated IMA performance will be evaluated and compared with the single IMU. To facilitate comparative analysis, the magnitude of navigation parameter estimation error is defined as [24],

$$\|\Delta x\| = \sqrt{\Delta x_E^2 + \Delta x_N^2 + \Delta x_U^2} \tag{29}$$

where Δx_E^2, Δx_N^2, Δx_U^2 represent the estimated error corresponding to the east, north, and up directions, respectively.

The attitude error, velocity error and position error of the IMA are compared with those of the single IMU. Note that we set the measurement noise covariance of the single IMU as one-fifth of that of the IMUs which make up the IMA, and this means the measurement accuracy of the single IMU is higher than that of the latter in the experimental comparison. Since the inertia height channel is unstable, the height error is omitted when the position error is compared in the experiment. The experiment results are shown in Fig. 8-10.

It can be seen from the above figures that the navigation parameters errors caused by the IMA is smaller than that caused by a single IMU during the flight of UAV. However, after a while, the error of the IMA will also be very large. This is owing to that the position of the UAV is obtained by integrating the acceleration twice, the navigation error is inevitably accumulated all the time.

3) THE ERROR COMPENSATION AND THE FINAL POSITIONING RESULTS

In this subsection, the GPS measurements are introduced into IMA for error compensation to form the complete three-layer

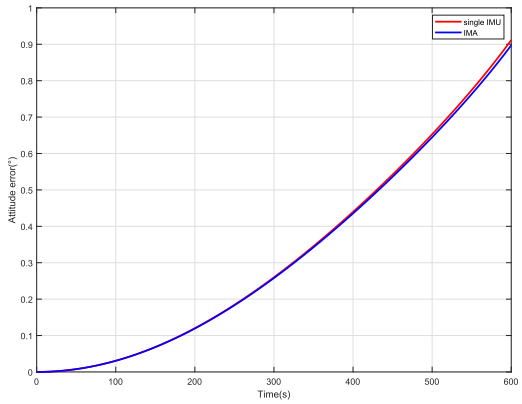

FIGURE 8. Comparison of attitude errors obtained by the single IMU and the IMA.

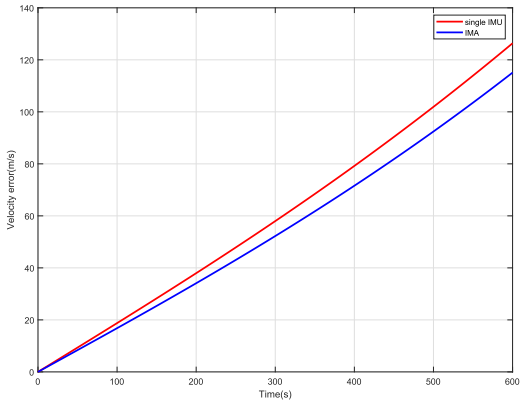

FIGURE 9. Comparison of velocity errors obtained by the single IMU and the IMA.

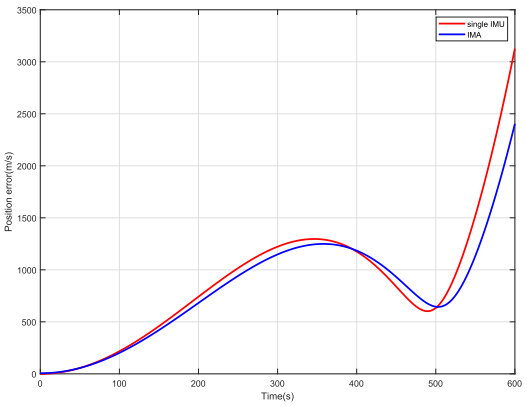

FIGURE 10. Comparison of position errors obtained by the single IMU and the IMA.

data fusion system. Comparing with GPS-aided single IMU and GPS, the proposed system can provide better positioning results.

The comparison results of the position error obtained by GPS-aided IMA before and after error compensation are shown in Fig. 11, which shows that after the error

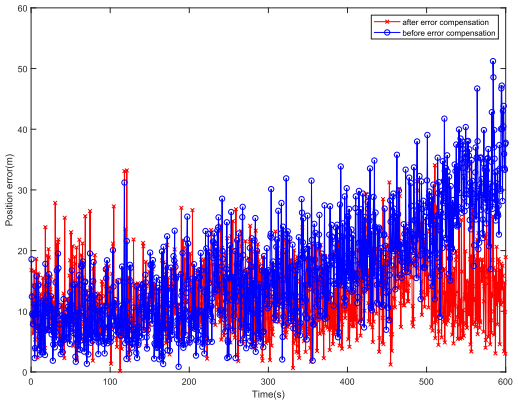

FIGURE 11. Comparison of position errors obtained by the GPS-aided IMA before and after error compensation.

compensation, the position error of the UAV does not continue to increase with time.

Finally, we compared the navigation errors of the UAV equipped with GPS, GPS-aided single IMU and GPS-aided IMA respectively. The experimental results are shown in Fig. 12-13.

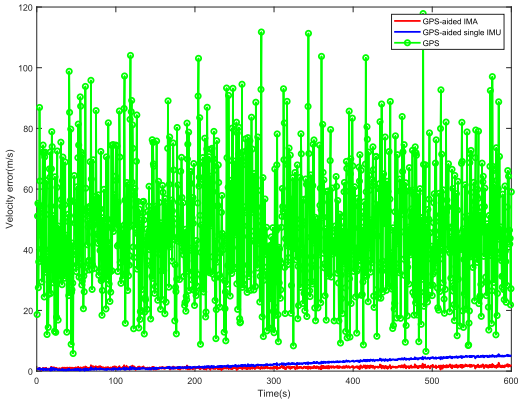

FIGURE 12. Comparison of velocity errors obtained by GPS-aided IMA, GPS-aided single IMU and GPS.

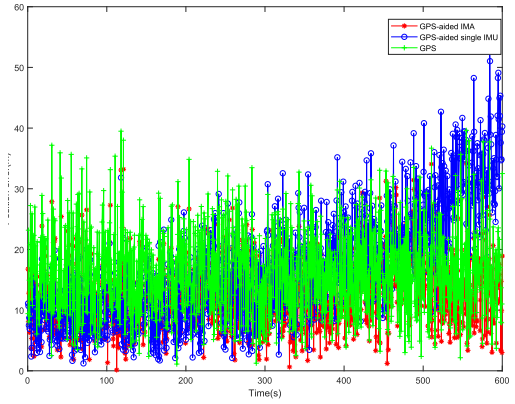

FIGURE 13. Comparison of position errors obtained by GPS-aided IMA, GPS-aided single IMU and GPS.

It can be seen from the above two pictures that the positioning accuracy of UAV using GPS-aided IMA is the highest among the three navigation methods. The Root Mean Squared Error (RMSE) of the positioning results corresponding to the three navigation methods is shown in Table 2.

TABLE 2. RMSE of the three navigation methods.

	GPS	GPS-aided single-IMU	GPS-aided IMA
Velocity	50.1183	2.8559	1.2754
Position	17.5023	19.4724	13.8255

IV. CONCLUSION

This paper has presented a novel positioning system of UAV based on IMA-GPS three-layer data fusion. This method has innovatively constructed a three-layer data fusion structure, which can effectively improve the accuracy and robustness of UAV positioning. The simulation results have shown that the proposed navigation system using GPS-aided IMA can improve the accuracy of UAV positioning and greatly improve the performance of the UAV positioning system compared with the navigation system using GPS-aided single IMU.

The future work will focus on the low dynamic motion, and the IMA will be considered to be combined with a camera for navigation and positioning, because the navigation accuracy of a camera is higher than that of the GPS in the low dynamic motion. We are also interested in the fault detection of IMA in the system. When one or more IMU in IMA failed, IMA can accurately detect the faulty unit and continue to complete the positioning function according to the information of the working IMU. In addition, we will also study on the Cramér-Rao Bound (CRLB) for the sensor fusion problem.

REFERENCES

[1] J. B. Gao and C. J. Harris, "Some remarks on Kalman filters for the multisensor fusion," *Inf. Fusion*, vol. 3, no. 3, pp. 191–201, Sep. 2002.

[2] S. Gao, Y. Zhong, X. Zhang, and B. Shirinzadeh, "Multi-sensor optimal data fusion for INS/GPS/SAR integrated navigation system," *Aerosp. Sci. Technol.*, vol. 13, nos. 4–5, pp. 232–237, Jun. 2009.

[3] B. Khaleghi, A. Khamis, F. O. Karray, and S. N. Razavi, "Multisensor data fusion: A review of the state-of-the-art," *Inf. Fusion*, vol. 14, no. 1, pp. 28–44, Jan. 2013.

[4] R. Gravina, P. Alinia, H. Ghasemzadeh, and G. Fortino, "Multi-sensor fusion in body sensor networks: State-of-the-art and research challenges," *Inf. Fusion*, vol. 35, pp. 68–80, May 2017.

[5] Y. Zhang, "A fusion methodology to bridge GPS outages for INS/GPS integrated navigation system," *IEEE Access*, vol. 7, pp. 61296–61306, 2019.

[6] G. Wang, X. Xu, Y. Yao, and J. Tong, "A novel BPNN-based method to overcome the GPS outages for INS/GPS system," *IEEE Access*, vol. 7, pp. 82134–82143, 2019.

[7] D. Li, X. Jia, and J. Zhao, "A novel hybrid fusion algorithm for low-cost GPS/INS integrated navigation system during GPS outages," *IEEE Access*, vol. 8, pp. 53984–53996, 2020.

[8] M. J. Choi, Y. H. Kim, E. J. Kim, and J. W. Song, "Enhancement of heading accuracy for GPS/INS by employing average velocity in low dynamic situations," *IEEE Access*, vol. 8, pp. 43826–43837, 2020.

[9] Y. Zhang, C. Shen, J. Tang, and J. Liu, "Hybrid algorithm based on MDF-CKF and RF for GPS/INS system during GPS outages (April 2018)," *IEEE Access*, vol. 6, pp. 35343–35354, 2018.

[10] H. Martin, P. Groves, M. Newman, and R. Faragher, "A new approach to better low-cost MEMS IMU performance using sensor arrays," in *Proc. 26th Int. Tech. Meeting Satell.-Division Inst. Navigat. (ION GNSS)*, Nashville, TN, USA, Sep. 2013, pp. 1–18.

[11] G. Panahandeh, I. Skog, and M. Jansson, "Calibration of the accelerometer triad of an inertial measurement unit, maximum likelihood estimation and Cramér-Rao bound," in *Proc. Int. Conf. Indoor Positioning Indoor Navigat.*, Sep. 2010, pp. 1–6.

[12] J.-O. Nilsson and I. Skog, "Inertial sensor arrays—A literature review," in *Proc. Eur. Navigat. Conf. (ENC)*, May 2016, pp. 1–10.

[13] R. Rasoulzadeh and A. M. Shahri, "Implementation of a low-cost multi-IMU hardware by using a homogenous multi-sensor fusion," in *Proc. 4th Int. Conf. Control, Instrum., Autom. (ICCIA)*, Jan. 2016, pp. 451–456.

[14] R. Rasoulzadeh and A. M. Shahri, "Accuracy improvement of a multi-MEMS inertial measurement unit by using an iterative UFIR filter," in *Proc. Eur. Navigat. Conf. (ENC)*, May 2017, pp. 279–286.

[15] H. Chang, L. Xue, C. Jiang, M. Kraft, and W. Yuan, "Combining numerous uncorrelated MEMS gyroscopes for accuracy improvement based on an optimal Kalman filter," *IEEE Trans. Instrum. Meas.*, vol. 61, no. 11, pp. 3084–3093, Nov. 2012.

[16] I. Skog, J.-O. Nilsson, and P. Handel, "An open-source multi inertial measurement unit (MIMU) platform," in *Proc. Int. Symp. Inertial Sensors Syst. (ISISS)*, Feb. 2014, pp. 1–4.

[17] J.-O. Nilsson, A. K. Gupta, and P. Handel, "Foot-mounted inertial navigation made easy," in *Proc. Int. Conf. Indoor Positioning Indoor Navigat. (IPIN)*, Oct. 2014, pp. 24–29.

[18] S. Bose, A. K. Gupta, and P. Handel, "On the noise and power performance of a shoe-mounted multi-IMU inertial positioning system," in *Proc. Int. Conf. Indoor Positioning Indoor Navigat. (IPIN)*, Sep. 2017, pp. 1–8.

[19] I. Skog, J.-O. Nilsson, P. Handel, and A. Nehorai, "Inertial sensor arrays, maximum likelihood, and Cramér–Rao bound," *IEEE Trans. Signal Process.*, vol. 64, no. 16, pp. 4218–4227, Aug. 2016.

[20] B. Gao, G. Hu, S. Gao, Y. Zhong, and C. Gu, "Multi-sensor optimal data fusion for INS/GNSS/CNS integration based on unscented Kalman filter," *Int. J. Control, Autom. Syst.*, vol. 16, no. 1, pp. 129–140, Feb. 2018.

[21] B. Gao, G. Hu, S. Gao, Y. Zhong, and C. Gu, "Multi-sensor optimal data fusion based on the adaptive fading unscented Kalman filter," *Sensors*, vol. 18, no. 2, p. 488, Feb. 2018.

[22] J.-O. Nilsson, I. Skog, and P. Handel, "Aligning the forces—Eliminating the misalignments in IMU arrays," *IEEE Trans. Instrum. Meas.*, vol. 63, no. 10, pp. 2498–2500, Oct. 2014.

[23] K. Xiong, L. D. Liu, and H. Y. Zhang, "Modified unscented Kalman filtering and its application in autonomous satellite navigation," *Aerosp. Sci. Technol.*, vol. 13, nos. 4–5, pp. 238–246, Jun. 2009.

[24] D. Wang, H. Lv, and J. Wu, "Augmented cubature Kalman filter for nonlinear RTK/MIMU integrated navigation with non-additive noise," *Measurement*, vol. 97, pp. 111–125, Feb. 2017.

[25] H. Qi and J. B. Moore, "Direct Kalman filtering approach for GPS/INS integration," *IEEE Trans. Aerosp. Electron. Syst.*, vol. 38, no. 2, pp. 687–693, Apr. 2002.

[26] Y. Y. Qin, "Strapdown inertial navigation system," in *Inertial Navigation*, 2nd ed. Beijing, China: Science Press, 2014, pp. 311–316.

[27] A. Noureldin, T. B. Karamat, M. D. Eberts, and A. El-Shafie, "Performance enhancement of MEMS-based INS/GPS integration for low-cost navigation applications," *IEEE Trans. Veh. Technol.*, vol. 58, no. 3, pp. 1077–1096, Mar. 2009.

[28] J. Zhang, T. Zhang, X. Jiang, and S. Wang, "Tightly coupled GPS/INS integrated navigation algorithm based on Kalman filter," in *Proc. 2nd Int. Conf. Bus. Comput. Global Informatization*, Oct. 2012, pp. 588–591.

[29] W. Hao, T. Lei, and R. Jian, "New approach for GPS/INS integrated navigation," in *Proc. 3rd Int. Symp. Intell. Inf. Technol. Appl. Workshops*, Nov. 2009, pp. 312–316.

[30] Y.-K. Kim, S.-H. Choi, and J.-M. Lee, "Enhanced outdoor localization of multi-GPS/INS fusion system using mahalanobis distance," in *Proc. 10th Int. Conf. Ubiquitous Robots Ambient Intell. (URAI)*, Oct. 2013, pp. 488–492.

[31] L. Tian, J. Rong, X. Zhong, and T. Li, "UPF algorithm and its application in the GPS/INS integrated navigation," in *Proc. Int. Conf. Wireless Commun. Signal Process.*, Nov. 2009, pp. 1–4.

[32] S. Huang, J. Huang, D. Tang, and F. Chen, "Research on UAV flight performance test method based on dual antenna GPS/INS integrated system," in *Proc. IEEE 3rd Int. Conf. Commun. Inf. Syst. (ICCIS)*, Dec. 2018, pp. 106–116.

[33] S. Z. Jamal, "Tightly coupled GPS/INS airborne navigation system," *IEEE Aerosp. Electron. Syst. Mag.*, vol. 27, no. 4, pp. 39–42, Apr. 2012.

YUAN WANG received the B.S. degree in automation from the University of Shanghai for Science and Technology, Shanghai, China, in 2018, where he is currently pursuing the M.S. degree with the School of Optical–Electrical and Computer Engineering. His research interests include simultaneous localization and mapping, and multi-sensor fusion.

GUOLIANG WEI (Member, IEEE) received the B.Sc. degree in mathematics from Henan Normal University, Xinxiang, China, in 1997, and the M.Sc. degree in applied mathematics and the Ph.D. degree in control engineering from Donghua University, Shanghai, China, in 2005 and 2008, respectively.

He was a Research Assistant with The University of Hong Kong, Hong Kong, in 2007, for two months, and the City University of Hong Kong, Hong Kong, in 2008, for two months. From 2009 to 2010, he was a Postdoctoral Research Fellow of the Department of Information Systems and Computing, Brunel University London, Uxbridge, U.K., sponsored by the Leverhulme Trust, U.K. From 2010 to 2011, he was an Alexander von Humboldt Research Fellow of the Institute for Automatic Control and Complex Systems, University of Duisburg–Essen, Duisburg, Germany. He is currently a Professor with the Department of Control Science and Engineering, University of Shanghai for Science and Technology, Shanghai. He has published over 50 articles in refereed international journals. His current research interests include nonlinear systems, stochastic systems, and bioinformatics.

Dr. Wei is a very active Reviewer for many international journals.

QI GUAN received the B.S. degree in electrical engineering and automation from the Qingdao University of Technology, Qingdao, China, in 2013, and the M.S. degree in control science and engineering from the University of Shanghai for Science and Technology, Shanghai, China, in 2018, where he is currently pursuing the D.E. degree with the School of Optical–Electrical and Computer Engineering.

His research interests include visual SLAM, multi-sensor fusion, and image processing and machine vision.

YANGYANG LIU received the B.S. degree in electronics and information engineering from Zaozhuang University, Zaozhuang, China, in 2018. He is currently pursuing the M.S. degree with the School of Optical–Electrical and Computer Engineering, University of Shanghai for Science and Technology. His research interests include visual SLAM and computer vision.